JFM RAPIDS
journals.cambridge.org/rapids

Compositional inhomogeneities as a source of indirect combustion noise

Luca Magri[1], **Jeff O'Brien**[1] **and Matthias Ihme**[1],†

[1]Center for Turbulence Research, Stanford University, 488 Escondido Mall, Stanford, CA 94305, USA

The generation of indirect combustion noise by compositional inhomogeneities is examined theoretically. For this, the compact-nozzle theory of Marble & Candel (*J. Sound Vib.*, vol. 55 (2), 1977, pp. 225–243) is extended to a multi-component gas mixture, and the chemical potential function is introduced as an additional acoustic source mechanism. Transfer functions for subcritical and supercritical nozzle flows are derived, and the contribution of compositional noise is compared to entropy noise and direct noise by considering an idealized nozzle downstream of the combustor exit. It is shown that compositional noise is dependent on the local mixture composition and can exceed entropy noise for fuel-lean conditions and supercritical nozzle flows. This suggests that the compositional indirect noise requires potential consideration with the implementation of low-emission combustors.

Key words: acoustics, combustion, gas dynamics

1. Introduction

The importance of engine-core noise as a relevant contributor to the overall noise emission from aircraft has been recognized, particularly for low-power engine conditions during landing and approach. Engine-core noise in aircraft gas turbines is commonly divided into direct and indirect noise (Strahle 1978; Candel *et al.* 2009; Dowling & Mahmoudi 2015). Direct combustion noise is a source of self-noise, and describes the generation of acoustic pressure fluctuations by unsteady heat release in the combustion chamber. In contrast, indirect combustion noise represents an induced noise-source mechanism that arises from the interaction between non-acoustic perturbations exiting the combustion chamber and downstream engine components. The indirect noise generation by temperature inhomogeneities arising from hot and cold spots is referred to as entropy noise (Candel 1972; Marble & Candel 1977), and indirect noise from vorticity fluctuations is referred to as vorticity noise (Cumpsty 1979). Once sound has been generated, its propagation through the engine

† Email address for correspondence: mihme@stanford.edu

core depends on mean-flow gradients and geometric properties, which distort, diffract and reflect the acoustics. An additional noise mechanism, which is commonly neglected in the core-noise analysis, results from the modulation of the jet-noise sources by mean-flow deformations and perturbations exiting the engine core (Ihme 2017).

Direct combustion noise was examined through experimental measurements to obtain fundamental understanding about the noise-source mechanisms and the effect of fuel mixtures and operating conditions on the acoustic radiation (Hurle *et al.* 1968; Singh *et al.* 2005), through theoretical analysis to determine the correlations for acoustic power, spectral density, and peak frequency (Rajaram & Lieuwen 2003; Candel *et al.* 2009), and through computational modelling using direct methods and acoustic analogies (Zhao & Frankel 2001; Ihme, Pitsch & Bodony 2009).

Contributions of indirect noise to the overall core-noise emission have been examined theoretically and experimentally. These studies focused on separating the contributions to noise from the direct transmission and entropy noise. Different techniques have been employed to determine the transfer functions, including the compact-nozzle theory (Marble & Candel 1977), the effective nozzle-length method (Stow, Dowling & Hynes 2002; Goh & Morgans 2011), linear nozzle element techniques (Moase, Brear & Manzie 2007; Giauque, Huet & Clero 2012), and expansion methods (Duran & Moreau 2013), among others. These theoretical investigations were supported by experimental studies. Bake *et al.* (2009) conducted measurements on an entropy-wave generator to investigate entropy noise by varying the mass flow rate, nozzle Mach number, heating power, and nozzle geometry. These investigations were extended by Kings & Bake (2010) to examine the indirect noise mechanisms arising from vorticity fluctuations. These studies showed that indirect combustion noise requires consideration in the analysis of engine-core noise and can exceed the contribution from direct noise.

Common to all of these previous theoretical and experimental investigations, however, is the restriction to a single-component gas mixture without considering effects of inhomogeneities in mixture composition on the indirect noise generation. In particular, compositional inhomogeneities can arise from incomplete mixing, air dilution, and variations in the combustor exhaust-gas compositions. The presence of compositional noise as an additional indirect noise-source mechanism was first identified analytically by Ihme (2017). The objective of the present work is to extend this analysis by quantifying the importance of this combustion noise mechanism in subcritical and supercritical nozzles. To this end, the equations for multi-component gas mixtures are considered, and compositional fluctuations are expressed as a function of the mixture fraction. Following Marble & Candel (1977), the compact-nozzle theory is used to derive transfer functions for different nozzle conditions. A parametric study is conducted to compare the relative contributions between compositional noise, entropy noise, and direct noise.

2. Theoretical analysis

The present analysis is concerned with the flow of a multi-component gas mixture through a nozzle. The following assumptions on the nozzle flow are made: (i) the flow is quasi-one-dimensional, i.e. the variables change because of area variations but depend only on the axial coordinate; (ii) the gas is ideal with frozen internal energy modes so that the heat capacity only depends on the mixture composition; (iii) the gas is composed of N_s species Y_i with chemical potentials μ_i; (iv) the flow is chemically

frozen, thus, all species are expressed in terms of mixture fraction, Z, $Y_i = Y_i(Z)$; (v) perturbations have a low frequency, i.e. the Helmholtz number is small, $He \ll 1$, therefore, the flow is quasi-steady and the compact-nozzle assumption is valid; (vi) the nozzle is isentropic except across the shock for the supercritical nozzle flow.

Assumptions (ii)–(iv) imply that the gas constant, R, is a function of the mixture fraction, because $R = \mathscr{R} \sum_{i=1}^{N_s} Y_i(Z)/W_i$, where W_i is the molar mass and $\mathscr{R}$ is the universal gas constant. Likewise, the specific heat capacity is a function of the mixture fraction, $c_p = \gamma/(\gamma - 1)R(Z)$, and γ is constant. The frozen-flow assumption (iv) is valid if the Damköhler number is small, i.e. $Da = \tau_{flow}/\tau_{chem} < 1$, where τ_{flow} is the flow time scale and τ_{chem} is the characteristic chemical time scale. This condition can be reformulated as $He/(M \omega \tau_{chem}) < 1$, where M is the Mach number and ω is the perturbation frequency. For expanding nozzle flows, the chemical time scale becomes large due to the reduction of the temperature and the reduced chemical reactivity of three-body recombination reactions (Keck & Gillespie 1971). Body forces, viscous-diffusive, Soret and Dufour effects are neglected due to the nozzle flow conditions at high Reynolds numbers.

2.1. *Governing equations*

In a multi-component chemically frozen gas, the differential of the total sensible enthalpy is defined as $\mathrm{d}h_t = \mathrm{d}h + u\,\mathrm{d}u$ and the sensible enthalpy is a function of species composition and temperature, $\mathrm{d}h = c_p\,\mathrm{d}T + \sum_{i=1}^{N_s} h_i\,\mathrm{d}Y_i$. With this and assumptions (i)–(v), the first-order perturbations of the total enthalpy, mass flow rate, and entropy read, respectively (Williams 1985),

$$\frac{\mathrm{d}h_t}{h_t} = \frac{2}{2 + (\gamma - 1)M^2} \left[\frac{\mathrm{d}T}{T} + (\gamma - 1)\frac{M}{c}\,\mathrm{d}u + \frac{c_p'}{c_p}\,\mathrm{d}Z \right], \qquad (2.1a)$$

$$\frac{\mathrm{d}\dot{m}}{\dot{m}} = \frac{\mathrm{d}\rho}{\rho} + \frac{\mathrm{d}u}{Mc}, \qquad (2.1b)$$

$$\frac{\mathrm{d}s}{c_p} = \frac{\mathrm{d}T}{T} - \frac{\gamma - 1}{\gamma}\frac{\mathrm{d}p}{p} + \left(\frac{c_p'}{c_p} - \Psi \right)\mathrm{d}Z, \qquad (2.1c)$$

where T is the temperature, u is the velocity, c is the speed of sound, ρ is the density, s is the entropy, p is the pressure, and γ is the ratio of specific heat capacities. The symbol $'$ denotes differentiation with respect to Z, i.e. $c_p' = \mathrm{d}c_p/\mathrm{d}Z$; $M = u/c$; Z is the mixture fraction; $\mu_i = \mu_i^0 + \mathscr{R}T \ln(p_i/p_0)$ is the chemical potential of the ith species (Job & Herrmann 2006). The superscript '0' denotes the standard condition, and $\Psi = (1/c_p T) \sum_{i=1}^{N_s} (\mu_i/W_i)Y_i'$ is the chemical potential function, comparing the chemical potential to the sensible enthalpy. Note that Ψ is a function of the thermochemical state, $\Psi = \Psi(p, T, Z)$; however, the dependency (p, T, Z) is dropped for brevity. The chemical potential is the partial derivative of the Gibbs function, G, with respect to the number of moles of the ith species, n_i, at constant temperature and pressure, i.e. $\mu_i = (\partial G/\partial n_i)_{T,p,n_{j \neq i}}$.

The conservation of mass, energy, entropy and species provides the set of governing equations, which are expressed as jump conditions across the compact nozzle

$$[\![\mathrm{d}\dot{m}]\!]_a^b = 0, \quad [\![\mathrm{d}h_T]\!]_a^b = 0, \quad [\![\mathrm{d}s]\!]_a^b = 0, \quad [\![\mathrm{d}Z]\!]_a^b = 0, \qquad (2.2a-d)$$

where the indices a and b denote the conditions at the inlet and outlet of the nozzle, respectively (figure 1). The system of governing equations is closed by the differential form of the state equation $\mathrm{d}p/p = \mathrm{d}\rho/\rho + (R'/R)\,\mathrm{d}Z + \mathrm{d}T/T$.
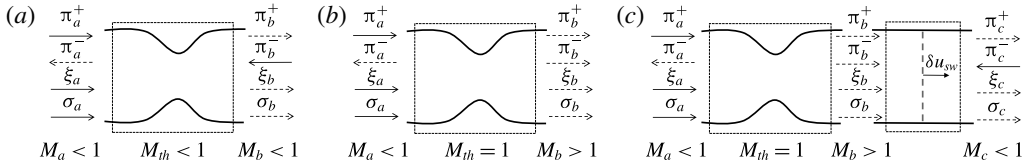
FIGURE 1. Acoustic, π, entropy, σ, and compositional, ξ, wave decomposition in a (*a*) subcritical nozzle, (*b*) supercritical nozzle and (*c*) supercritical nozzle with a normal shock wave. Incoming waves are denoted by solid arrows; outgoing waves are denoted by dashed arrows. In the compact-nozzle assumption, the nozzles are viewed as black boxes, depicted as dashed boxes, with properties evaluated at the inlet, *a*, and outlet, *b*. The flow region downstream of the shock wave is labelled *c*. M_{th} is the Mach number at the throat.

The jump conditions (2.2) combined with the state equation provide five relations for the five unknowns dp, dρ, dT, du and dZ. The entropy, ds, can be used as an alternative thermodynamic variable through the Gibbs relation (2.1*c*). Furthermore, R' and Y_i', appearing in the derivative of c_p and the definition of Ψ, are not state variables, because they depend on the chemical composition, which will be discussed in §3. In a choked nozzle, the variables are constrained by the condition that the mass flow rate attains a maximum, $\dot{m}^* = \sqrt{\gamma}A_{th}p_t/(\sqrt{RT_t})[(\gamma + 1)/2]^{-(\gamma+1)/[2(\gamma-1)]}$, where the superscript $*$ indicates the sonic condition and the subscript '*th*' denotes the condition at the throat. Equating the sonic mass flow rate to the mass flow rate (2.1*b*), $\mathrm{d}\dot{m}^*/\dot{m}^* = \mathrm{d}\dot{m}/\dot{m} = 0$ yields the additional condition

$$\frac{\mathrm{d}s}{2c_p} + \frac{1}{2}\Psi\,\mathrm{d}Z - \frac{\mathrm{d}u}{Mc} + \frac{\gamma-1}{2\gamma}\frac{\mathrm{d}p}{p} = 0. \tag{2.3}$$

The left-hand side of (2.3) is equal to the perturbation Mach number, $\mathrm{d}M = \mathrm{d}u/c - M\,\mathrm{d}c/u$, where $\mathrm{d}c = c/2[(R'/R)\,\mathrm{d}Z + \mathrm{d}T/T]$, which, therefore, is zero throughout the compact choked nozzle.

2.2. *Nozzle transfer functions*

In the linear limit, the acoustic pressure mode is governed by a wave equation, whereas entropy and mixture-fraction modes are governed by convection equations (when the species diffusion is neglected). Extending the fundamental mode decomposition of Chu & Kovásznay (1958) to the mixture fraction, it is inferred that these three modes are decoupled. Therefore, a characteristic decomposition can be employed. Hence, four independently evolving waves at each side of the nozzle are identified, as shown in figure 1, which correspond to the downstream and upstream propagating acoustic waves, the convective entropy wave and the convective compositional wave, respectively,

$$\pi^{\pm} = \frac{1}{2}\left(\frac{\mathrm{d}p}{\gamma p} \pm \frac{\mathrm{d}u}{c}\right), \quad \sigma = \frac{\mathrm{d}s}{c_p}, \quad \xi = \mathrm{d}Z. \tag{2.4a-c}$$

A nozzle transfer function is defined as the ratio between a single output, such as an outgoing acoustic wave, and a single input, such as an incoming entropy or compositional wave. The objective is to derive analytical transfer-function expressions for the indirect noise by compositional fluctuations, which is done by considering a subcritical nozzle, a supercritical nozzle, and a supercritical nozzle with a normal shock.

	Subcritical nozzle	Supercritical nozzle
π_b^+/π_a^+	$\dfrac{2(1+M_a)M_b}{(1+M_b)(M_a+M_b)}\dfrac{\left[2+(\gamma-1)M_b^2\right]}{\left[2+(\gamma-1)M_aM_b\right]}$	$\dfrac{2+(\gamma-1)M_b}{2+(\gamma-1)M_a}$
π_b^+/σ_a	$\dfrac{(M_b-M_a)M_b}{(1+M_b)\left[2+(\gamma-1)M_aM_b\right]}$	$\dfrac{1}{2}\dfrac{M_b-M_a}{2+(\gamma-1)M_a}$
π_b^+/ξ_a	$\dfrac{(\gamma-1)(\Psi_b-\Psi_a)\left[2+(\gamma-1)M_b^2\right]M_aM_b}{(\gamma-1)(1+M_b)(M_a+M_b)[2+(\gamma-1)M_aM_b]}$ $+\dfrac{M_b[2(\Psi_a-\Psi_b)+(\gamma-1)(\Psi_aM_b^2-\Psi_bM_a^2)]}{(\gamma-1)(1+M_b)(M_a+M_b)[2+(\gamma-1)M_aM_b]}$	$\dfrac{1}{2(\gamma-1)}\left[\dfrac{2+(\gamma-1)M_b}{2+(\gamma-1)M_a}\Psi_a-\Psi_b\right]$

TABLE 1. Transfer functions for subcritical and supercritical nozzles. The transfer functions π_b^+/π_a^+ and π_b^+/σ_a were derived by Marble & Candel (1977).

2.2.1. *Subcritical nozzle*

Using the wave decomposition (2.4) and noting that $\sigma_a=\sigma_b=\sigma$ and $\xi_a=\xi_b=\xi$, the linearized equations for enthalpy and mass flow rate, (2.1a) and (2.1b), can be written as

$$\frac{\mathrm{d}h_t}{h_t}=\frac{2(\gamma-1)}{2+(\gamma-1)M^2}\left[(1+M)\pi^+ +(1-M)\pi^- +\frac{\sigma+\Psi\xi}{\gamma-1}\right], \qquad (2.5a)$$

$$\frac{\mathrm{d}\dot{m}}{\dot{m}}=\left(1+\frac{1}{M}\right)\pi^+ +\left(1-\frac{1}{M}\right)\pi^- -\sigma-\Psi\xi. \qquad (2.5b)$$

Substituting (2.5) into (2.2) provides a linear set of algebraic equations that relates the four incoming waves $(\pi_a^+,\sigma_a,\xi_a,\pi_b^-)$ to the four outgoing waves $(\pi_a^-,\sigma_b,\xi_b,\pi_b^+)$. After algebraic manipulations, the transfer functions between the acoustic wave leaving the nozzle and the acoustic, entropy, and compositional waves entering the nozzle can be derived (Ihme 2017), and the resulting expressions are presented in table 1.

2.2.2. *Supercritical nozzle*

For a supercritical nozzle flow (figure 1b), the inputs are three incoming waves (π_a^+,σ_a,ξ_a) and the outputs are five outgoing waves $(\pi_a^-,\sigma_b,\xi_b,\pi_b^+,\pi_b^-)$. Similar to the subcritical nozzle, $\sigma_a=\sigma_b=\sigma$ and $\xi_a=\xi_b=\xi$ due to the jump conditions (2.2). As explained in §2.1, the perturbation of the mass flow rate provides two conditions

$$\sigma+\Psi_a\xi+\left[\frac{M_a(\gamma-1)-2}{M_a}\right]\pi_a^+ +\left[\frac{M_a(\gamma-1)+2}{M_a}\right]\pi_a^-=0, \qquad (2.6a)$$

$$\sigma+\Psi_b\xi+\left[\frac{M_b(\gamma-1)-2}{M_b}\right]\pi_b^+ +\left[\frac{M_b(\gamma-1)+2}{M_b}\right]\pi_b^-=0. \qquad (2.6b)$$

By relating outgoing and ingoing waves, the transfer functions are obtained and are summarized in table 1. The relations for the outgoing wave π_b^-, needed in §2.2.3, can be derived by antisymmetry, substituting $M_b\rightarrow-M_b$ into the transfer functions for π_b^+.

2.2.3. *Supercritical nozzle with shock wave*

It is assumed that the pressure at the nozzle exit is such that a shock wave occurs downstream of the choked condition. The disturbances $(\pi_b^+, \pi_b^-, \sigma, \xi)$ impinge on the shock wave and move its position by a first-order perturbation to the velocity, δu_{sw} (figure 1*c*). To calculate the outgoing waves downstream of the shock wave (π_c^+, σ_c), noting that $\xi_c = \xi$ because the flow is frozen, the following procedure is implemented (Marble & Candel 1977). First, the flow variables are expressed in the reference frame attached to the shock wave by a Galilean transformation $u_b - \delta u_{sw}$ and $u_c - \delta u_{sw}$, which defines the effective Mach number $M_{b,sw} = M_b(1 - \delta u_{sw}/u_b)$. Second, the Rankine–Hugoniot relations for velocity, pressure and density are linearized by considering the linearized effective Mach number, $dM_{b,sw} = dM_b - M_b \delta u_{sw}/u_b$, where $dM_b = 0$ for a choked flow (see (2.3)) and $dM_b \delta u_{sw}$ is neglected because it is of higher order. These read, respectively,

$$\frac{du_c}{u_c} - \frac{du_b}{u_b} = \frac{u_b}{u_c} \left[\frac{4}{(\gamma + 1) M_b^2} - \frac{u_c}{u_b} + 1 \right] \frac{\delta u_{sw}}{u_b}, \tag{2.7a}$$

$$\frac{dp_c}{\gamma p_c} - \frac{dp_b}{\gamma p_b} = -\frac{p_b}{p_c} \frac{4M_b^2}{(\gamma + 1)} \frac{\delta u_{sw}}{u_b}, \tag{2.7b}$$

$$\frac{d\rho_c}{\rho_c} - \frac{d\rho_b}{\rho_b} = -\frac{\rho_b}{\rho_c} \frac{(\gamma + 1) M_b^2}{\left[1 + \frac{1}{2} (\gamma - 1) M_b^2 \right]^2} \frac{\delta u_{sw}}{u_b}. \tag{2.7c}$$

Equations (2.7*a*), along with the linearized continuity equation, provide the perturbed flow state after the shock wave (du_c, dp_c, $d\rho_c$) and the shock-wave velocity, δu_{sw}. Finally, the wave decomposition (2.4) and Gibbs relation for the density, $d\rho/\rho = dp/(\gamma p) - ds/c_p - \Psi \, dZ$ are applied. With this, the outgoing acoustic and entropy waves after the shock read, respectively,

$$\pi_c^+ = \left(\frac{1 + 2M_c^2 M_b + M_b^2}{1 + 2M_b^2 M_c + M_b^2} \right) \pi_b^+ + \left(\frac{1 - 2M_c^2 M_b + M_b^2}{1 + 2M_b^2 M_c + M_b^2} \right) \pi_b^-, \tag{2.8a}$$

$$\sigma_c = \sigma - (\Psi_c - \Psi_b)\xi + \left[\frac{(\gamma - 1)(M_b^2 - 1)^2}{M_b^2(2 + (\gamma - 1)M_b^2)} \right] (\pi_c^+ + \pi_c^- - \pi_b^+ - \pi_b^-). \tag{2.8b}$$

Note that u_c, p_c and ρ_c in (2.7) depend on the Mach number downstream of the shock wave, M_c, which, in turn, is related to the Mach number upstream of the shock wave, M_b, through the normal shock-wave relation

$$M_c^2 = \frac{M_b^2(\gamma - 1) + 2}{2\gamma M_b^2 - (\gamma - 1)}. \tag{2.9}$$

The transfer functions π_c^+/π_a^+, π_c^+/σ_a and π_c^+/ξ_a can be derived by substituting the transfer functions for π_b^+ and π_b^- for a choked nozzle into (2.8*a*). It is interesting to note that the difference in the chemical potential function in (2.8*b*), $(\Psi_c - \Psi_b)\xi$, is a further source of entropy across the shock wave.

2.3. *Comments on the theoretical analysis*

The indirect noise generated by compositional inhomogeneities is physically due to the transfer of chemical potential energy into acoustic energy through the accelerating flow. From the transfer functions and transmission relations that were derived in the

previous sections, the following limits are worth considering. First, when $M_a \rightarrow M_b$, the compositional noise tends to zero because $\Psi_a \rightarrow \Psi_b$ (table 1). Second, in the limit of a constant chemical potential function, $\Psi_a = \Psi_b$, it can be shown that the ratio between compositional noise and entropy noise for all the three cases tends to the same limit Ψ. This limit physically signifies that the indirect noise ratio is independent of the flow conditions, and is only a function of the thermodynamic and compositional state at the inlet, under the compact-nozzle assumption.

3. Results

The analysis developed in the previous section is applied to a flow-path configuration to quantify the relative contribution of compositional noise to the overall combustion noise. For this, we consider an idealized configuration in which the combustor exhaust-gas composition enters the nozzle. This exhaust-gas composition is represented by the solution of a series of one-dimensional strained diffusion flames (Peters 2000) that include the equilibrium composition, typically observed at low-power cruise conditions, and highly strained combustion conditions representative of high-load operation. The flame solutions are generated by considering *n*-dodecane ($C_{12}H_{26}$), a kerosene surrogate, as fuel and air in the oxidizer stream at operating conditions of 295 K and ambient pressure. The flame structure is parameterized by the mixture fraction, with $Z = 0$ corresponding to the oxidizer stream and $Z = 1$ corresponding to the pure fuel stream. The flame structure is obtained from the steady-state solution of the conservation equations for continuity, species, and energy, which are solved using the CANTERA software package (Goodwin, Moffatt & Speth 2016). The reaction chemistry is described by a 24-species mechanism (Vie *et al.* 2015), which provides an accurate flame representation at these conditions.

The degree of straining, i.e. the deviation from equilibrium, is characterized by the scalar dissipation rate, $\chi = 2\alpha|\nabla Z|^2$, where α is the diffusivity of the mixture fraction, and χ is evaluated at the stoichiometric condition, corresponding to a value of $Z_{st} = 0.063$. Large values of χ_{st} correspond to high-strain-rate conditions, in which the diffusive transport of heat away from the flame exceeds the heat release. Flame extinction occurs when χ_{st} exceeds the quenching limit. The present study considers three flames with different conditions. The structure of each of these flames, together with the chemical potential function and the specific Gibbs energy, are shown in figure 2 for (a,d) $\chi_{st} = 0.1$ s^{-1} (quasi-unstrained condition near equilibrium), (b,e) $\chi_{st} = 21$ s^{-1} (intermediately strained flame condition), and (c,f) $\chi_{st} = 50$ s^{-1} (highly strained flame at condition near extinction). The results are presented as a function of the transformed mixture-fraction coordinate $Z/(Z + Z_{st})$, which divides the plot evenly between lean ($Z < Z_{st}$) and rich ($Z > Z_{st}$) conditions.

These flame solutions can be interpreted as an idealized representation of the gas composition exiting the combustor. The combustor operates at a global equivalence ratio ϕ, corresponding to a mean mixture fraction Z, with $Z = \phi Z_{st}/[Z_{st}(\phi - 1) + 1]$ (Peters 2000). The corresponding thermochemical state is then taken from the flame solution of figure 2. In addition to temperature fluctuations, which are known to generate entropy noise, incomplete mixing, turbulence, and other unsteady effects give rise to fluctuations in Z. This has the potential to produce compositional noise downstream of the combustor. To assess the compositional noise that is generated, the combustor exhaust composition for a given value of Z is isentropically compressed through an ideal nozzle, keeping the mean mixture composition frozen at this flame state. Since gas-turbine combustors typically operate at subsonic conditions, without
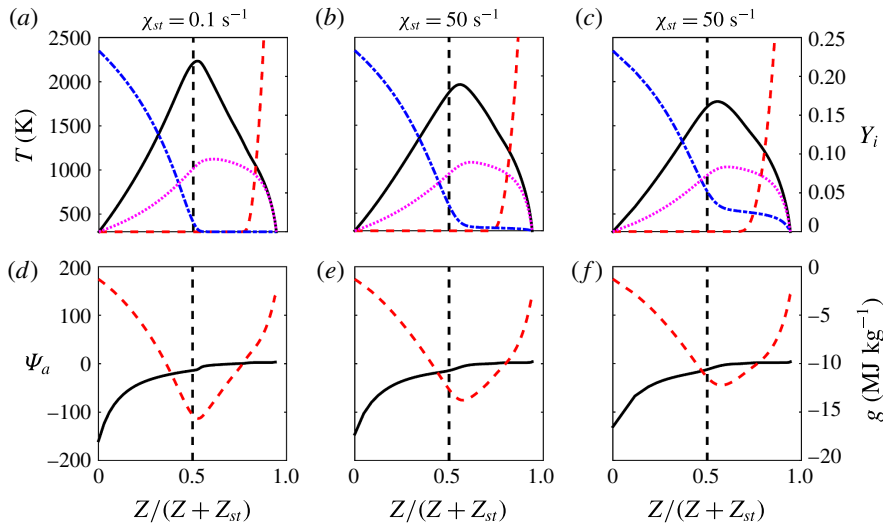
FIGURE 2. Representation of one-dimensional diffusion flame in mixture-fraction composition space for three different scalar dissipation rates. (a,d) $\chi_{st} = 0.1$ s^{-1} (quasi-unstrained condition near equilibrium), (b,e) $\chi_{st} = 21$ s^{-1} (intermediately strained flame condition), and (c,f) $\chi_{st} = 50$ s^{-1} (highly strained flame at condition near extinction). $(a$–$c)$ Flame structure, showing temperature T (solid black lines), oxygen mass fraction Y_{O_2} (blue dot-dashed lines), n-dodecane mass fraction $Y_{C_{12}H_{26}}$ (red dashed lines), and water mass fraction Y_{H_2O} (magenta dotted lines). $(d$–$f)$ Chemical potential function Ψ_a (solid black lines) and specific Gibbs energy of the mixture, $g = \sum_i (\mu_i / W_i) Y_i$ (dashed red lines). Z_{st} is the stoichiometric mixture fraction. Operating conditions: $C_{12}H_{26}$/air combustion, $T_{fuel} = T_{ox} = 295$ K, $p = 1$ bar.

loss of generality, it is assumed that $M_a = 0$. The transfer functions of table 1 and the shock-wave case (§ 2.2.3) are then evaluated over the full mixture-fraction space and a range of relevant nozzle-exit Mach numbers.

The transfer-function ratios between compositional noise, direct noise, and entropy noise for different nozzle flows and combustor exhaust compositions are presented in figure 3. Figures 3$(a$–$c)$ and 3$(d$–$f)$ show the ratio of the transfer functions between compositional and direct noise and between compositional and entropy noise, respectively, for an ideally expanded nozzle. Figure 3$(g$–$l)$ shows the corresponding results for the nozzle flow with shock wave.

From these results, it can be seen that the transfer function for the compositional noise depends on nozzle-exit condition, gas composition and dissipation rate. This is most pronounced for fuel-lean and supersonic conditions. The dependence of the compositional noise on the gas mixture at fuel-lean conditions is particularly noteworthy because it corresponds to the typical operating regime of modern gas-turbine engines. This sensitivity is a direct result of stronger variations of the mixture composition and inherent differences in the chemical potential at fuel-lean conditions. This suggests that variations in the equivalence ratio, for instance during the engine operation, or the consideration of low-emission combustor concepts, can lead to noise modulation by induced compositional noise, in addition to direct and entropy noise.

Effects of increasing scalar dissipation rate are mainly evident for fuel-lean conditions, which is attributed to the leakage of reactants and incomplete combustion,
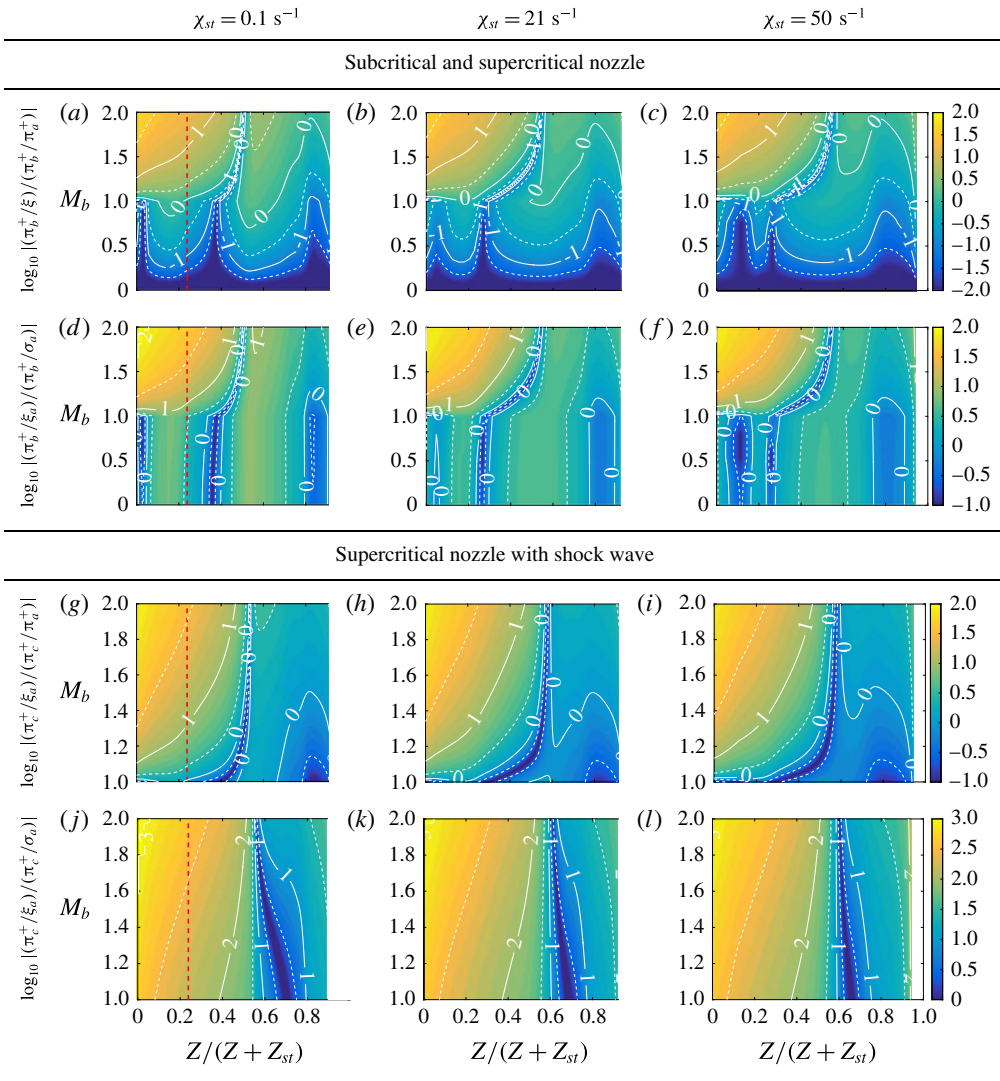
FIGURE 3. Transfer-function ratios for (*a*–*c*) compositional noise to direct noise; (*d*–*f*) compositional noise to entropy noise; (*g*–*i*) compositional noise to direct noise after a shock wave; and (*j*–*l*) compositional noise to entropy noise after a shock wave. The columns correspond to the three combustor exit conditions of figure 2. The vertical red dashed line indicates the condition of an equivalence ratio of $\phi = 0.3$.

thereby reducing the chemical potential function. Figure 2 shows the variation of the chemical potential function as well as the specific Gibbs energy as a function of the mixture fraction. It can be seen that the variation in g, and correspondingly the magnitude of Ψ, are largest at fuel-lean conditions. While this broadening effect is most easily seen in physical space, it also has a weaker sensitivity in mixture-fraction space, leading to the differences with respect to χ_{st}. Simulations at higher pressure conditions show that the pressure has a secondary effect on the magnitude of the transfer function (results not shown). This is likely because

differences in the chemical potential vary weakly with the temperature and pressure because the chemical composition of the flame is not strongly changing along these paths, and the chemical potential depends logarithmically on the pressure. At extreme temperatures and pressures, where dissociation of diatomic gases occurs, the sensitivity to the thermodynamic state is likely to be much stronger.

To connect these results to practical applications, we provide an estimate of the ratio of composition noise to entropy noise by multiplying the corresponding transfer-function ratios with the factor $\xi_a/\sigma_a = \delta Z_a/(\delta T_a/T_a)$. This factor is estimated by considering that the mixture composition at the combustor exit reaches equilibrium with a mean temperature of $T_a = 1085$ K, corresponding to an equivalence ratio of $\phi_a = 0.3$ and mean mixture fraction of $Z_a = 0.0197$ at the condition shown in figure 2(*a*). The mixture-fraction distribution at the combustor exit is represented, to a first approximation, by a beta-distribution, $\beta(z)$. The fluctuation magnitude is estimated as $\delta Z_a = \sqrt{\zeta Z_a(1 - Z_a)}$, where $\zeta \in [0, 1]$ is a coefficient for the mixedness (Dimotakis & Miller 1990). In a combustor in which the mixing is nearly completed with $\zeta = 10^{-4}$, the temperature fluctuation can be evaluated from $\delta T_a = \{\int_0^1 [T(z) - T_a]^2 \beta(z)\,\mathrm{d}z\}^{1/2}$, where $T(z)$ is the flame solution from figure 2(*a*). Hence, one finds that $\xi_a/\sigma_a = 0.015$, indicating that the noise ratio at subsonic condition is below 0.1. However, this ratio increases to values of 0.5 (supercritical nozzle) and exceeds values of 5 (supercritical nozzle with shock), as shown by the red dashed lines in figure 3. This suggests that the compositional noise can become a relevant contributor to indirect combustion noise at these conditions.

4. Conclusions and discussion

By modelling inhomogeneities in the gas composition exiting the combustor and entering a nozzle, the compositional noise is identified as a source of indirect combustion noise. To describe this source mechanism, the compact-nozzle theory is extended to consider a multi-component gas mixture and the chemical potential function. This theory is applied to subcritical and supercritical nozzle flows. It is found that the compositional noise exhibits a strong dependence on the mixture composition, and can become comparable to – and even exceed – direct noise and entropy noise for supercritical nozzles and lean mixtures. This suggests that compositional noise may require consideration with the implementation of low-emission combustors, high-power-density engine cores, or compact burner concepts (Hultgren 2011; Chang, Lee, Herbon & Kramer 2013).

The present analysis employed the compact-nozzle theory, which relies on simplifications that are not strictly valid for $He > 0$ (see § 2). Therefore, the compact-nozzle assumption can be relaxed to consider effects of finite nozzle-length and wave phase differences, as discussed in § 1. In addition, multi-dimensional high-fidelity numerical simulations provide further opportunities to assess the importance of compositional noise, which is the subject of ongoing research.

This analysis also stipulates the need for experimental investigations to measure compositional noise and obtain a firm evaluation of the level of compositional inhomogeneities at the combustor exit in gas-turbine engines. Since the product species of CO_2, H_2O, and CO are leading contributors to the chemical potential function, gas-sampling probes, tunable diode laser absorption spectroscopy, and other intrusive and non-intrusive techniques, could be employed to quantify the spatial and temporal evolution of compositional inhomogeneities.

Acknowledgement

References

BAKE, F., RICHTER, C., MÜHLBAUER, C., KINGS, N., RÖHLE, I., THIELE, F. & NOLL, B. 2009 The entropy wave generator (EWG): a reference case on entropy noise. *J. Sound Vib.* **326**, 574–598.

CANDEL, S. M. 1972 Analytical studies of some acoustic problems of jet engines, PhD thesis, California Institute of Technology.

CANDEL, S., DUROX, D., DUCRUIX, S., BIRBAUD, A.-L., NOIRAY, N. & SCHULLER, T. 2009 Flame dynamics and combustion noise: progress and challenges. *Intl J. Aeroacoust.* **8** (1–2), 1–56.

CHANG, C. T., LEE, C.-M., HERBON, J. T. & KRAMER, S. K. 2013 NASA environmentally responsible aviation project develops next-generation low-emissions combustor technologies (Phase I). *J. Aeronaut. Aerosp. Engng* **2** (4), 1000116.

CHU, B. T. & KOVÁSZNAY, L. S. G. 1958 Non-linear interactions in a viscous heat-conducting compressible gas. *J. Fluid Mech.* **3**, 494–514.

CUMPSTY, N. A. 1979 Jet engine combustion noise: pressure, entropy and vorticity perturbations produced by unsteady combustion or heat addition. *J. Sound Vib.* **66** (4), 527–544.

DIMOTAKIS, P. E. & MILLER, P. L. 1990 Some consequences of the boundedness of scalar fluctuations. *Phys. Fluids* **2** (11), 1919–1920.

DOWLING, A. P. & MAHMOUDI, Y. 2015 Combustion noise. *Proc. Combust. Inst.* **35**, 65–100.

DURAN, I. & MOREAU, S. 2013 Solution of the quasi-one-dimensional linearized Euler equations using flow invariants and the Magnus expansion. *J. Fluid Mech.* **723**, 190–231.

GIAUQUE, A., HUET, M. & CLERO, F. 2012 Analytical analysis of indirect combustion noise in subcritical nozzles. *Trans. ASME: J. Engng Gas Turbines Power* **134** (111202), 1–8.

GOH, C. S. & MORGANS, A. S. 2011 Phase prediction of the response of choked nozzles to entropy and acoustic disturbances. *J. Sound Vib.* **330**, 5184–5198.

GOODWIN, D. G., MOFFATT, H. K. & SPETH, R. L. 2016 CANTERA: An object-oriented software toolkit for chemical kinetics, thermodynamics, and transport processes. Version 2.2.1. http://www.cantera.org.

HULTGREN, L. S. 2011 Core noise: implications of emerging $N+3$ designs and acoustic technology needs. *Acoustics Technical Working Group, Cleveland, OH, USA*.

HURLE, I. R., PRICE, R. B., SUGDEN, T. M. & THOMAS, A. 1968 Sound emission from open turbulent premixed flames. *Proc. R. Soc. Lond.* A **303**, 409–427.

IHME, M. 2017 Combustion and engine-core noise. *Annu. Rev. Fluid Mech.* **49** (in press); doi:10.1146/annurev-fluid-122414-034542.

IHME, M., PITSCH, H. & BODONY, D. 2009 Radiation of noise in turbulent non-premixed flames. *Proc. Combust. Inst.* **32**, 1545–1553.

JOB, G. & HERRMANN, F. 2006 Chemical potential – a quantity in search of recognition. *Eur. J. Phys.* **27** (2), 353–371.

KECK, J. C. & GILLESPIE, D. 1971 Rate-controlled partial-equilibrium method for treating reacting gas mixtures. *Combust. Flame* **17**, 237–241.

KINGS, N. & BAKE, F. 2010 Indirect combustion noise: noise generation by accelerated vorticity in a nozzle flow. *Intl J. Spray Combust. Dyn.* **2** (3), 253–266.

MARBLE, F. E. & CANDEL, S. M. 1977 Acoustic disturbance from gas non-uniformities convected through a nozzle. *J. Sound Vib.* **55** (2), 225–243.

MOASE, W. H., BREAR, M. J. & MANZIE, C. 2007 The forced response of choked nozzles and supersonic diffusers. *J. Fluid Mech.* **585**, 281–304.

PETERS, N. 2000 *Turbulent Combustion*. Cambridge University Press.

RAJARAM, R. & LIEUWEN, T. 2003 Parametric studies of acoustic radiation from premixed flames. *Combust. Sci. Technol.* **175** (12), 2269–2298.

SINGH, K. K., ZHANG, C., GORE, J. P., MONGEAU, L. & FRANKEL, S. H. 2005 An experimental study of partially premixed flame sound. *Proc. Combust. Inst.* **30**, 1707–1715.

STOW, S. R., DOWLING, A. P. & HYNES, T. P. 2002 Reflection of circumferential modes in a choked nozzle. *J. Fluid Mech.* **467**, 215–239.

STRAHLE, W. C. 1978 Combustion noise. *Prog. Energy Combust. Sci.* **4**, 157–176.

VIE, A., FRANZELLI, B., GAO, Y., LU, T., WANG, H. & IHME, M. 2015 Analysis of segregation and bifurcation in turbulent spray flames: a 3D counterflow configuration. *Proc. Combust. Inst.* **35** (2), 1675–1683.

WILLIAMS, F. A. 1985 *Combustion Theory*. Perseus Books.

ZHAO, W. & FRANKEL, S. H. 2001 Numerical simulations of sound radiated from an axisymmetric premixed reacting jet. *Phys. Fluids* **13** (9), 2671–2681.